RESEARCH ACTIVITIES II
Department of Molecular Structure

II-A Development of Dynamic Near-Field Spectroscopy and Application to Nanometric Systems

There is much demand for the study of local optical properties of molecular assemblies and materials, to understand mesoscopic phenomena and/or to construct optoelectronic devices in the nanometric scale. Scanning near-field optical microscopy (SNOM), which enables spatial resolution beyond the diffraction limit of light, shows remarkable progress in technology in these days. Combination of this advanced optical technology with ultrafast spectroscopic methods may offer a direct probe of molecular dynamical processes in mesoscopic systems. It may bring essential and basic knowledge for analyzing origins of characteristic features and functionalities of mesoscopic systems. We are constructing apparatuses for near-field dynamic spectroscopy with the femtosecond temporal resolution and the nanometer spatial resolution. Using the apparatuses developed, we have observed characteristic spatiotemporal behavior of various organic molecular systems and metal nanoparticles, for the purpose of understanding spatial coherence and dissipation of excitations and their dynamics. Outlines of the experimental results obtained are summarized here.

II-A-1 Morphological and Spectroscopic Properties of Thin Films of Self-Assembling Amphiphilic Porphyrins on Hydrophilic Surface as Revealed by Scanning Near-Field Optical Microscopy

NAGAHARA, Tetsuhiko; IMURA, Kohei; OKAMOTO, Hiromi; OGURO, Akane[1]; IMAHORI, Hiroshi[1]
([1]Kyoto Univ.)

[*J. Phys. Chem. B* **109**, 19839–19844 (2005)]

We fabricated porphyrin thin films on mica surfaces from acidic aqueous solutions of the pre-organized H-aggregates of amphiphilic porphyrins (5,10,15,20-tetrakis(4-(4-(trimethylammonio)butoxy)phenyl) porphyrin bromide, TABPP, and the related compounds) by simple spin-coating method. The morphological and spectroscopic properties of the film formed on mica substrate were investigated by atomic force microscopy and scanning near-field optical microscopy. The surface topographic image and the near-field transmission image taken at the wavelength of the H-aggregate band (Figures 1a and b) are negatively correlated very well each other. That is, the optical transmission at the position of higher topographic height (the bright part in the topographic image) is lower than that at the lower-height position. This indicates that the film of ~3 nm height consists mainly of the H-aggregate. The results obtained demonstrate that the pre-organized H-aggregate structure in solution can be transferred as a thin film with a thickness of monolayer level without losing their substantial structure and photophysical properties.

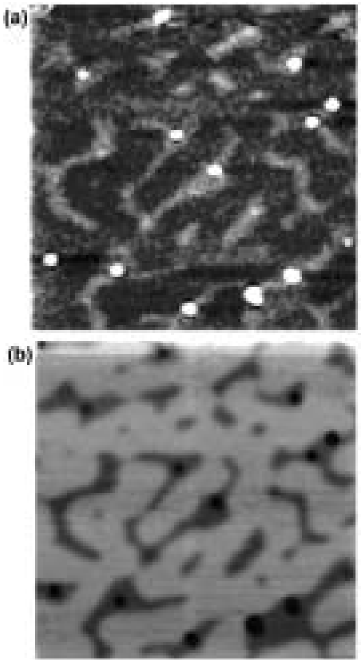

Figure 1. (a) Surface topography of the thin-film sample of TABPP on mica (scan area: 10 μm × 10 μm × 3 nm). Bright and dark parts correspond to high and low parts of the sample surface, respectively. (b) Transmission image of the sample obtained at 430 nm. Bright and dark parts correspond to high and low transmission intensities, respectively.

II-A-2 Scanning Near-Field Optical Microscopic Study of Porphyrin Nanowire

NAGAHARA, Tetsuhiko; IMURA, Kohei; OKAMOTO, Hiromi; OZAWA, Hiroaki; OGAWA, Takuji

We studied optical properties of molecular nanowires of coupled zinc porphyrins with bulky dendric groups, by means of scanning near-field optical microscopy and spectroscopy. The topographic images and the near-field-excited fluorescence images gave string-like structures, and correlated well to each other. We also performed polarization dependence measurements. The analysis of the obtained data is now in progress.

II-A-3 Imaging of Plasmon Modes in Gold Nanorods

IMURA, Kohei; NAGAHARA, Tetsuhiko; OKAMOTO, Hiromi

[*J. Phys. Chem. B* **109**, 13214–13220 (2005)]

Surface plasmon resonances (SPRs) of noble metals have attracted much interest, since the SPR gives not only fundamental importance in science but also various applications in nanotechnology. Knowledge of the spatial characteristics of the surface plasmons, as well as the spectral and polarization characteristics, is essential for the control of electric field confinement in near-field and of plasmon properties. We investigate the spatial characteristics of plasmon-mode wavefunctions by a SNOM.

Gold nanorods were prepared in solutions using the seed-mediated methods. For SNOM measurements, gold nanorods were dispersed on cover-slips by spin-coating method. Figures 1(a,b) show two typical near-field two-photon induced photoluminescence (TPI-PL) images observed for single gold nanorods. The dotted squares indicate approximate shapes of the rods estimated from the topographic measurements. As can be seen in the figures, the PL intensities show characteristic spatial oscillations along the long axis. Figures 1(c,d) show calculated electromagnetic local density of states (LDOS) images for the corresponding nanorods. The good agreements between the observations and the calculated LDOS images indicate that oscillatory structures found in Figures 1(a,b) represent spatial characteristics of the plasmon modes of the nanorods at the excitation wavelength.

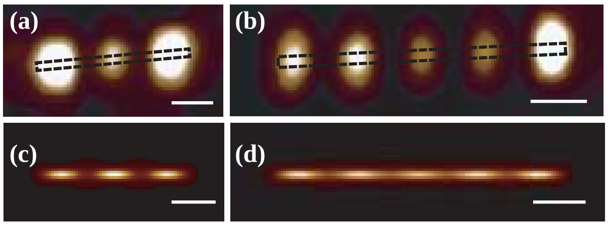

Figure 1. (a,b) TPI-PL images for single gold nanorods: (a) 20±5 nm × 330±30 nm, (b) 20±5 nm × 540±40 nm. (c,d) Calculated LDOS maps for the corresponding gold nanorods (a,b), respectively. Scale bars are 100 nm.

II-A-4 Near-Field Two-Photon Induced Photoluminescence from Single Gold Nanorods

IMURA, Kohei; NAGAHARA, Tetsuhiko; OKAMOTO, Hiromi

[*J. Phys. Chem. B* **109**, 13214–13220 (2005)]

Studies of photoluminescence (PL) from the metal nanoparticles were limited because of very low quantum efficiencies. A strong enhancement of PL from gold nanorods upon single photon excitation was reported.$^{1)}$ The enhancement was ascribed to the local field enhancement due to the SPR of the gold nanorods. Two-photon optical processes involve an additional field enhancement, and thus a greater enhancement of PL efficiency is expected. We investigate two-photon induced PL (TPI-PL) from single gold nanorods of variety of lengths and diameters using an apertured SNOM, in order to characterize the emission mechanism and the optical features of the TPI-PL process.

Dependencies of the PL intensity on the polarizations of both the excitation (incoming) and the emitted (outgoing) photons are shown in Figure 1. The dependence of the PL intensity on the incident electric-field polarization [Figure 1(a)] indicates that TPI-PL is excited by the sequential one-photon process. Figures 1(c) and 1(d) show polarization characteristics of the emitted photons from the X (645–655 nm) and L (450–550 nm) regions, respectively. The emission from the X region shows an almost perfect polarization along the long axis while that from the L region is only partially polarized. The polarization characteristics obtained can be reasonably understood on the basis of the crystalline structure and the band structure of the gold nanorods.

Reference

1) M. B. Mohamed, V. Volkov, S. Link and M. A. El-Sayed, *Chem. Phys. Lett.* **317**, 517 (2000).

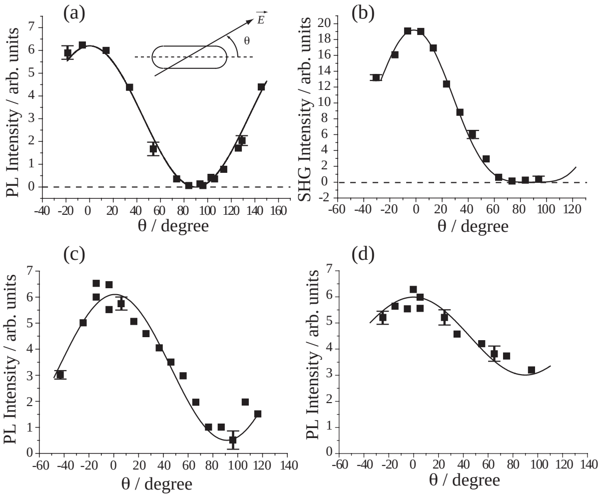

Figure 1. (a) Incident polarization dependence of the PL intensity. (b) Incident polarization dependence of the SHG intensity from the same nanorod. (c,d) Polarization characteristics of the detected photons in (c) the X region (645–655 nm) and (d) the L region (450–550 nm), respectively.

II-A-5 Dispersion Relation of Plasmon Modes in the Gold Nanorods

IMURA, Kohei; NAGAHARA, Tetsuhiko; OKAMOTO, Hiromi

[*J. Chem. Phys.* **122**, 154701 (2005)]

Surface plasmon (SP) resonaces of noble metal particles have recently attracted much interest, especially for their ability in local confinement of optical near-field. Imaging of electromagnetic local density of states (LDOS) inside single noble particles leads to direct optical observation of the SP modes. We study the optical-frequency dependent spatial characteristics of the LDOS inside the gold nanorods by the transmission-mode SNOM to obtain a dispersion relation of the SP modes.

By plotting the resonance frequencies of SP modes versus the wave vectors (which are directly obtained from the SP-mode images), the dispersion relation of the gold nanorod is obtained. The dispersion relation based on the DOS calculations for the rods is given in Figure 1 (triangles). The calculated points roughly follow a singe dispersion curve, which is converging to the resonace frequency of the transverse SP mode at high wavenumber limit. We have also found that the near-field observations for various length nanorods with approximately the same diameter (closed circles) follow this curve. The results indicate that the resonace energies of multipolar SP modes in various rods of a given diameter can be estimated from the dispersion curve, even if the rod lengths are different.

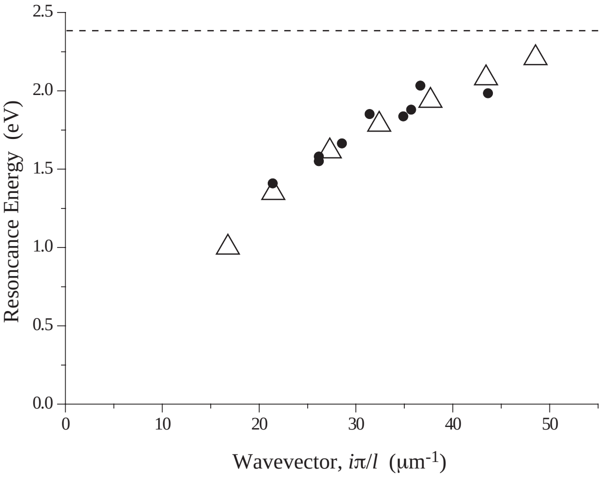

Figure 1. SP dispersion relation for gold nanorods. Closed circles: Observations. Open triangles: Calculations. Dashed horizontal line indicates the transverse SP resonance energy.

II-A-6 Imaging and Dispersion Relations of Surface Plasmon Modes in Silver Nanorods by Near-Field Spectroscopy

LIM, Jong Kuk[1]; IMURA, Kohei; NAGAHARA, Tetsuhiko; KIM, Seong Keun[2]; OKAMOTO, Hiromi
([1]IMS and Seoul Natl. Univ.; [2]Seoul Natl. Univ.)

[*Chem. Phys. Lett.* **412**, 41–45 (2005)]

Surface plasmons of silver nanorods were investigated by using scanning near-field optical microscopy. The silver nanorods were synthesized in water solution by reducing $AgNO_3$ under existence of surfactant molecules. Near-field transmission images showed spatially oscillatory patterns in the silver nanorods. The oscillatory features of images are attributable to plasmon-mode wavefunctions. As is similar to the gold nanorod cases, the spatial oscillation period depends on the wavelength of the observing light. From the near-field images and spectra, the wave vectors and the resonant frequencies of the plasmon modes observed were directly estimated. In this way the dispersion relations of the plasmon modes for various silver nanorods were obtained. It was found that dispersion relation of a nanorod is dependent on its diameter. The spectral features obtained are compared with those for gold nanorods.

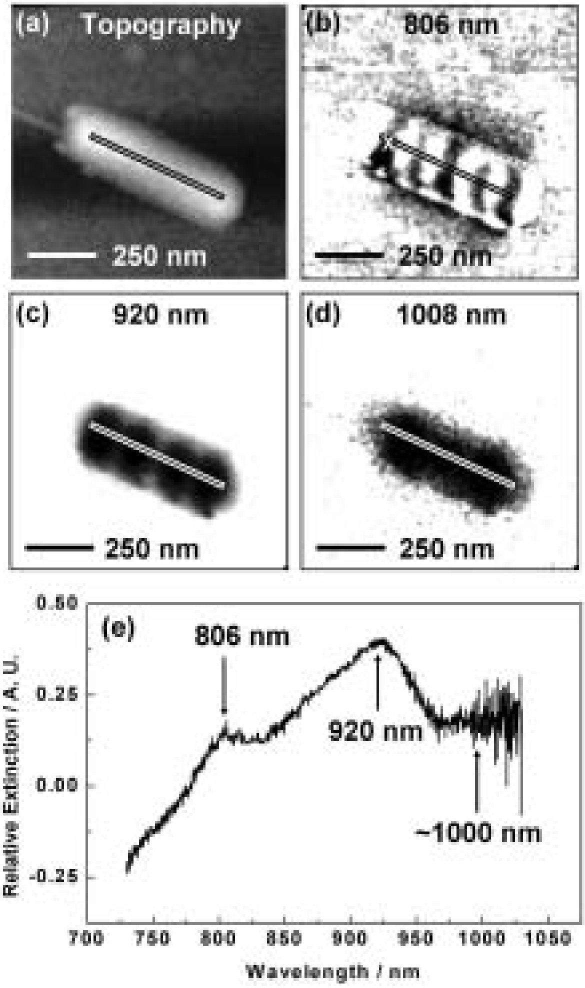

Figure 1. Representative images of nanorods and their near-field spectrum. (a) Topography of silver nanorod, *ca.* 20 nm in diameter and *ca.* 530 nm in length. (b)–(d) Near-field transmission images probed with an unpolarized light at 806, 920, and 1008 nm, respectively. (e) Near-field spectrum taken at the position marked “X” in the near-field transmission (b).

II-A-7 Ultrafast Near-Field Imaging of Single Gold Nanorods and Nanoplates

IMURA, Kohei; OKAMOTO, Hiromi

It is of fundamental importance to know how the electron-electron and electron-phonon scattering processes after photoexcitation depend upon size and shape of nanoparticles and how they proceed inside the particle. Dynamic spectroscopy of a single particle with high temporal and spatial resolution must be informative for this purpose. Previously we performed ultrafast near-field pump-probe imaging of relatively short gold nanorods, and revealed the position dependent electron-phonon relaxation. In the present study, we have extended the study to longer nanorods and nanoparticles of other shapes, and investigated the dynamic behavior after photoexcitation in a space- and time-resolved manner.

A Ti:sapphire laser (λ = 780 nm, < 100 fs, 80 MHz) was used for time-resolved pump-probe measurements. From the near-field pump-probe measurements of various single gold nanorods and nanoplates, we found that the energy dispassion processes are dependent upon its size and shape, as well as upon the internal position of the nanoparticle.

II-A-8 Near-Field Spectroscopy of Close-Packed Self-Assembled Monolayer Films of Gold Nanoparticles

IMURA, Kohei; OKAMOTO, Hiromi; HOSSAIN, M. Kamal[1]; ISHIOKA, Kunie[1]; KITAJIMA, Masahiro[1]
([1]Natl. Inst. Mater. Sci. and Univ. Tsukuba)

Two-dimensional (2D) nanostructured materials of noble metal nanoparticles, in particular gold nanoparticles, have attracted much attention because of their unique optical properties. To characterize its optical properties as well as its potentiality in industry, we are studying the transmission, two-photon induced photoluminescence (TPI-PL), and surface enhanced Raman scattering (SERS) from the 2D structure by near-field spectroscopy and microscopy.

The 2D nanostructure of gold nanoparticles was fabricated by simply controlling the surface tension and the coverage area. The surface morphology of the fabricated 2D structure was examined by an atomic force microscope and a scanning electron microscope, and found to be a well-ordered close-packed monolayer, whose area is as large as several hundreds μm^2 to mm^2.

In the near-field transmission spectra, it is found that the 2D structure exhibits several longitudinal surface plasmon resonances resulted from the localized plasmon coupling. In these regions, near-field TPI-PL and SERS intensities from the 2D structure are stronger than those from the isolated particles. These observations can be ascribed to the higher electric field enhancements in the ordered structure.

II-B Spectroscopic Studies on Atoms and Ions in Liquid Helium

Atoms and ions in liquid helium are known to reside in bubble-like cavities due to the Pauli repulsive force between electrons. Physical properties of these exotic surroundings are determined by the potential energy of the impurity-He$_n$ system, the surface tension energy of the liquid helium, and the pressure-volume work. Spectroscopic studies of such impurity atoms and ions in liquid helium are expected not only to give interesting information on the structure and dynamics of the bubbles but also to contribute to the study on physical properties of superfluid liquid helium.

II-B-1 Laser Spectroscopic Studies of Mg Atoms in Pressurized Liquid Helium

MORIWAKI, Yoshiki[1]; MORITA, Norio
([1]Toyama Univ.)

We have measured excitation and emission spectra of the 3s^2 ^{1}S$_0$–3s3p ^{1}P$_1$ transition of Mg atom in pressurized liquid helium-4 and helium-3. We have found that all these spectra show large spectral widths and large peak shifts with respect to the transition wavelength of free Mg atoms; while the excitation spectra are shifted toward the blue side, the emission spectra toward the red side. Although these are well-known spectral properties for impurity atoms in liquid He, we have also found that the peak wavelengths of the emission spectra, in particular, remain constant or slightly increase with the increasing liquid pressure. The latter is an interesting spectral property peculiar to this transition of Mg, because, for other atoms, such as Ba, Rb, Cs, Tm and Ca, and for other transitions of Mg, the increase of the liquid pressure always shifts their emission spectra toward shorter wavelength. Our bubble model calculation has successfully reproduced these properties of the Mg spectra, and has given a reasonable explanation to those peculiar properties. Moreover, further considerations based on the calculated results have suggested the possibility of the formation of a Mg(3s3p ^{1}P$_1$)He$_n$ exciplex in a bubble.

II-C Magnetic Structures of Magnetic Thin Films Studied by Using a Depth-Resolved XMCD Technique

Recently, we have developed a depth-resolved x-ray magnetic circular dichroism (XMCD) technique. In the soft x-ray region, an x-ray absorption spectrum is obtained generally by counting the Auger electrons emitted at the core hole relaxation, the number of which is proportional to the x-ray absorption intensity. The electron escape depth changes depending on the direction of emitted electrons. An imaging type microchannel plate is used as the electron detector, which enables us to collect the absorption spectra with various probing depths simultaneously. The XMCD spectra are obtained by reversing the sample magnetization direction at each incident helicity.

This simple technique can be applied to study the depth profile of magnetic structures of magnetic thin films.

II-C-1 Direct Observation of an Oscillatory Behavior in the Surface Magnetization of Fe Thin Films Grown on a Ni/Cu(100) Film

AMEMIYA, Kenta[1]; MATSUMURA, Daiju[1]; ABE, Hitoshi[1]; KITAGAWA, Soichiro[1]; OHTA, Toshiaki[2]; YOKOYAMA, Toshihiko
([1]Univ. Tokyo; [2]IMS and Univ. Tokyo)

[*Phys. Rev. B* **70**, 195405 (2004)]

When a Fe film is deposited on a ferromagnetic (FM) substrate, the interface (bottom) of the Fe film should undergo some magnetic interaction with the substrate. Our aim is to study the magnetic coupling between the surface and interface for the Fe films on 6 ML Ni/Cu(100) as a function of the Fe film thickness with the depth-resolved XMCD technique. Figure 1 shows Fe L-edge XMCD spectra from 4–11 ML Fe films grown on a 6 ML Ni/Cu(100) taken at 200 K with various probing depths, λ_e. Each spectrum was normalized to the edge jump height, so that the XMCD intensity reflects the magnetic moments per atom as an average over the contribution from each Fe layer weighted with the electron attenuation factor. A series of the spectra from the 4 ML film (region I) show almost identical intensity regardless of λ_e, directly indicating a simple ferromagnetic structure. In contrast, the XMCD intensity from the 4.5 ML film is drastically reduced as λ_e increases. Moreover, the XMCD spectra exhibit a positive sign at L_3 edge, indicating that the Fe surface has an opposite magnetization direction with respect to the applied filed. As the Fe thickness increases, the XMCD intensity decreases and almost vanishes around 6 ML, then grows up to 9 ML with an opposite sign. Finally, the XMCD signal almost disappears above 10 ML. These results clearly show that the Fe surface magnetization direction changes as a function of Fe thickness. Assuming that the magnetization of the Fe films consists of the contributions from (1) surface two layers, (2) inner layer and (3) interface layer, observed depth-resolved XMCD spectra were analyzed. The results show that the interface layer gives almost constant magnetization parallel with that of Ni, and the inner layer is almost nonmagnetic, and the surface two layers give the oscillatory magnetization depending on the Fe thickness. This apparent oscillation might come from the rotation of magnetic moment at the surface.

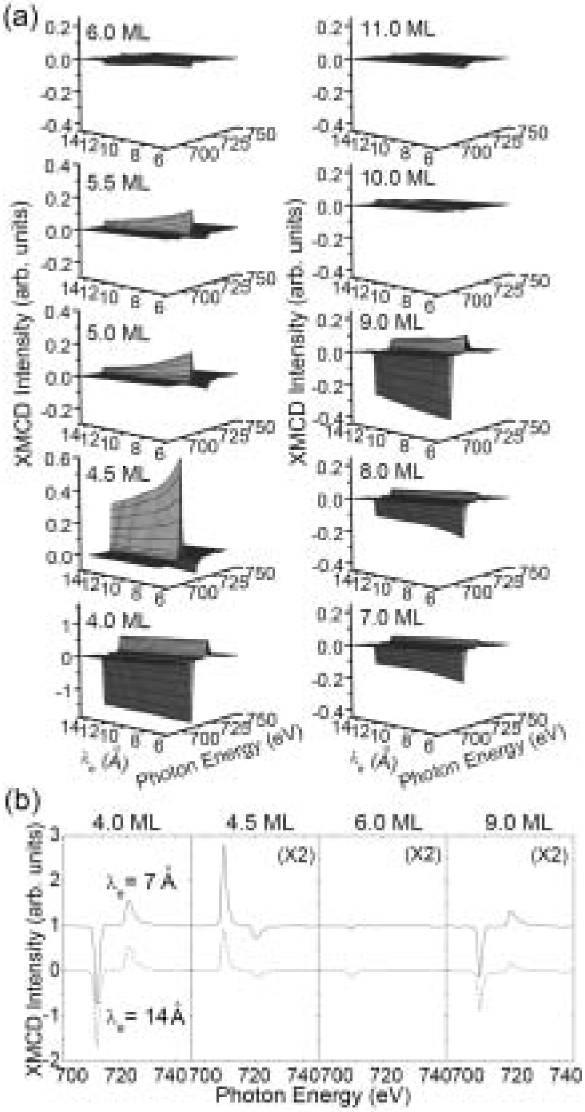

Figure 1. Fe L-edge XMCD spectra from Fe (4-11 ML)/Ni (6 ML)/Cu(100) films taken at 200 K with various probing depths, λ_e (a), together with the selected spectra at λ_e = 7 and 14 Å (b).

II-C-2 Spin Reorientation Transition of Ni/Cu(100) and CO/Ni/Cu(100): Separation of the Surface and Bulk Components of the X-Ray Magnetic Circular Dichroism Spectrum

AMEMIYA, Kenta[1]; SAKAI, Enju[1]; MATSUMURA, Daiju[1]; ABE, Hitoshi[1]; OHTA, Toshiaki[2]; YOKOYAMA, Toshihiko
([1]Univ. Tokyo; [2]IMS and Univ. Tokyo)

[*Phys. Rev. B* **71**, 214420 (2005)]

The spin reorientation transition of Ni/Cu(100) and CO/Ni/Cu(100) films was investigated with the depth-resolved x-ray magnetic circular dichroism (XMCD) technique. The XMCD spectra from the surface and inner layers were separately extracted. As for the bare Ni films, the in-plane orbital magnetic moment in the surface layer is significantly enhanced. In contrast, the inner layers exhibit larger perpendicular orbital magnetic moment than the in-plane one. Upon CO adsorption, the surface magnetization is drastically reduced, while the inner layers are unaffected. These results directly explain the spin reorientation transition mechanism in Ni/Cu(100) and CO/Ni/Cu(100) systems.

II-D Structure and Function of Metalloproteins and Its Molecular Design

Metal ion is a common cofactor that is crucial for active centers of proteins involved in many biologically important processes in cells, and a relatively small number of metal-based prosthetic groups are utilized to serve numerous and diverse chemical functions. A typical metal-based prosthetic group, which represents a fascinating example in this respect, is heme. Heme promotes a variety of functions, such as dioxygen storage, activation of small molecules, electron transfer reactions, and sensing gaseous molecule. In the field of protein design and engineering, hemoproteins also make particularly attractive targets. There are many reasons for this, including the exciting possibility of engineering protein-based molecules with useful catalytic, electronic or optoelectronic properties. Based on various kinds of spectroscopies, we have functionally and structurally characterized some hemoproteins including newly identified heme-regulated proteins, and designed hemoproteins showing improved activities and new functions.

II-D-1 L358P Mutation on P450cam Simulates Structural Changes upon Putidaredoxin Binding. The Structural Changes Trigger Electron Transfer to Oxy-P450cam from Electron Donors

TOSHA, Takehiko[1]; YOSHIOKA, Shiro[1]; ISHIMORI, Koichiro[2]; MORISHIMA, Isao[1]
([1]Kyoto Univ.; [2]IMS and Kyoto Univ.)

[*J. Biol. Chem.* **279**, 42836–42843 (2004)]

To investigate the functional and structural characterization of a crucial cytochrome P450cam (P450cam)-putidaredoxin (Pdx) complex, we utilized a mutant whose spectroscopic property corresponds to the properties of the wild type P450cam in the presence of Pdx. The ^{1}H NMR spectrum of the carbonmonoxy adduct of the mutant, the Leu-358 3 Pro mutant (L358P), in the absence of Pdx showed that the ring current-shifted signals arising from D-camphor were upfield-shifted and observed as resolved signals, which are typical for the wild type enzyme in the presence of Pdx. Signals from the β-proton of the axial cysteine and the γ-methyl group of Thr-252 were also shifted upfield and downfield, respectively, in the L358P mutant as observed for Pdx-bound wild type P450cam. The close similarity in the NMR spectra suggests that the heme environment of the L358P mutant mimics that of the Pdx-bound enzyme. The functional analysis of the L358P mutant has revealed that the oxygen adduct of the L358P mutant can promote the oxygenation reaction for D-camphor with nonphysiological electron donors such as dithionite and ascorbic acid, showing that oxygenated L358P is “activated” to receive electron from the donor. Based on the structural and functional characterization of the L358P mutant, we conclude that the Pdx-induced structural changes in P450cam would facilitate the electron transfer from the electron donor, and the Pdx binding to P450cam would be a trigger for the electron transfer to oxygenated P450cam.

II-D-2 Structural Diversities of Active Site in Clinical Azole Bound Forms between Sterol 14α-demethylases (CYP51) from Human and *Mycobacterium tuberculosis*

MATSUURA, Koji[1]; YOSHIOKA, Shiro; TOSHA, Takehiko; HORI, Hiroshi[2]; ISHIMORI, Koichiro[3]; KITAGAWA, Teizo; MORISHIMA, Isao[1]; KAGAWA, Norio[4]; WATERMAN, Michael R.[4]
([1]Kyoto Univ.; [2]Osaka Univ.; [3]IMS, Kyoto Univ. and Hokkaodo Univ.; [4]Vanderbilt Univ.)

[*J. Biol. Chem.* **280**, 9088–9096 (2005)]

To gain insights into the molecular basis of the design for the selective azole anti-fungals, we compared the binding properties of azole-based inhibitors for cytochrome P450 sterol 14α-demethylase (CYP51) from human (HuCYP51) and *Mycobacterium tuberculosis* (MtCYP51). Spectroscopic titration of azoles to the CYP51s revealed that HuCYP51 has higher affinity for ketoconazole (KET), an azole derivative that has long lipophilic groups, than MtCYP51, but the affinity for fluconazole (FLU), which is a member of the antifungal armamentarium, was lower in HuCYP51. The affinity for 4-phenylimidazole (4-PhIm) to MtCYP51 was quite low compared with that to HuCYP51. In the resonance Raman spectra for HuCYP51, the FLU binding induced only minor spectral changes, whereas the prominent high frequency shift of the bending mode of the heme vinyl group was detected in the KET- or 4-PhIm-bound forms. On the other hand, the bending mode of the heme propionate group for the FLU-bound form of MtCYP51 was shifted to high frequency as found for the KET-bound form, but that for 4-PhIm was shifted to low frequency. The EPR spectra for 4-PhIm-bound MtCYP51 and FLUbound HuCYP51 gave multiple g values, showing heterogeneous binding of the azoles, whereas the single g_x and g_z values were observed for other azole-bound forms. Together with the alignment of the amino acid sequence, these spectroscopic differences suggest that the region between the B’ and C helices, particularly the hydrophobicity of the C helix, in CYP51s plays primary roles in determining strength of interactions with azoles; this differentiates the binding specificity of azoles to CYP51s.

II-D-3 Two Heme Binding Sites Are Involved in the Regulated Degradation of the Bacterial Iron Response Regulator (Irr) Protein

YANG, Jianhua[1]; ISHIMORI, Koichiro[2]; O'BRIAN, Mark R.[1]
([1]New York State Univ.; [2]IMS and Kyoto Univ.)

[*J. Biol. Chem.* **280**, 7671–7676 (2005)]

The iron response regulator (Irr) protein from *Bradyrhizobium japonicum* is a conditionally stable protein that degrades in response to cellular iron availability. This turnover is heme-dependent, and rapid degradation involves heme binding to a heme regulatory motif (HRM) of Irr. Here, we show that Irr confers iron-dependent instability on glutathione *S*-transferase (GST) when fused to it. Analysis of Irr-GST derivatives with C-terminal truncations of Irr implicated a second region necessary for degradation, other than the HRM, and showed that the HRM was not sufficient to confer instability on GST. The HRM-defective mutant IrrC29A degraded in the presence of iron but much more slowly than the wild-type protein. This slow turnover was heme-dependent, as discerned by the stability of Irr in a heme-defective mutant strain. Whereas the HRM of purified recombinant Irr binds ferric (oxidized) heme, a second site that binds ferrous (reduced) heme was identified based on spectral analysis of truncation and substitution mutants. A mutant in which histidines 117–119 were changed to alanines severely diminished ferrous, but not ferric, heme binding. Introduction of these substitutions in an Irr-GST fusion stabilized the protein *in vivo* in the presence of iron. We conclude that normal iron-dependent Irr degradation involves two heme binding sites and that both redox states of heme are required for rapid turnover.

II-D-4 Involvement of Heme Regulatory Motif in Heme-Mediated Ubiquitination and Degradation of IRP2

ISHIKAWA, Haruto[1]; KATO, Michihiko[2]; HORI, Hiroshi[3]; ISHIMORI, Koichiro[4]; KIRISAKO, Takayoshi[2]; TOKUNAGA, Fuminori[2]; IWAI, Kozuhiro[2]
([1]Osaka City Univ.; [2]Osaka City Univ. and CREST; [3]Osaka Univ.; [4]IMS, Kyoto Univ., CREST and Hokkaodo Univ.)

[*Mol. Cell.* **19**, 171–181 (2005)]

Iron regulatory protein 2 (IRP2), a regulator of iron metabolism, is modulated by ubiquitination and degradation. We have shown that IRP2 degradation is triggered by heme-mediated oxidation. We report here that not only Cys201, an invariant residue in the heme regulatory motif (HRM), but also His204 is critical for IRP2 degradation. Spectroscopic studies revealed that Cys201 binds ferric heme, whereas His204 is a ferrous heme binding site, indicating the involvement of these residues in sensing the redox state of the heme iron and in generating the oxidative modification. Moreover, the HRM in IRP2 has been suggested to play a critical role in its recognition by the HOIL-1 ubiquitin ligase. Although HRMs are known to sense heme concentration by simply binding to heme, the HRM in IRP2 specifically contributes to its oxidative modification, its recognition by the ligase, and its sensing of iron concentration after iron is integrated into heme.

II-E Structure and Energy Changes during Protein Reaction Dynamics

The thermodynamic properties (enthalpy, thermal expansion coefficient, compressibility, partial molar volume, *etc.*) as well as the transport property (diffusion coefficient) of proteins are of fundamental importance to understand the structural fluctuation and the dynamics of protein molecules. Traditional techniques that can access to these quantities are certainly useful and powerful to characterize the proteins. However, knowledge of these properties of time-dependent or unstable (intermediate) species during biological reactions is very limited. It is most desirable to develop and use a method that can measure these properties in time domain so that reaction intermediates can be characterized in a similar way. In this project, we try to construct a method to probe energies and conformational changes as well as the diffusion coefficients of biological proteins in time domain. One of interesting applications of this technique is to detect spectral silent kinetics in reactions of biological proteins.

II-E-1 Hydrogen Bonding Dynamics During Protein Folding of Reduced Cytochrome *c*: Temperature and Denaturant Concentration Dependence

NISHIDA, Shinpei[1]; NADA, Tomokazu[1]; TERAZIMA, Masahide[2]
([1]Kyoto Univ.; [2]IMS and Kyoto Univ.)

[*Biophys. J.* **89**, 2004–2010 (2005)]

Folding dynamics of reduced cytochrome *c* triggered by the laser induced reduction method is investigated from a view point of the intermolecular interaction change. Change of the diffusion coefficient of Cyt *c* during the refolding process is traced in time domain from the unfolded value to the native value continuously at various denaturant (guanidine hydrochloride (GdnHCl)) concentrations and temperatures. In the temperature range of 288 K–308 K and GdnHCl concentration range of 2.5 M–4.25 M, the diffusion change can be analyzed well by the two state model consistently. It was found that the $m^{\ddagger}$-value and the activation energy of the transition state from the unfolded state for the hydrogen bonding network change are surprisingly similar to that for the local structural change around the heme group monitored by the fluorescence quenching experiment. This agreement suggests the existence of common or similar fundamental dynamics including water molecular movement to control the refolding dynamics. The nature of the transition state is discussed.

II-E-2 Conformational Dynamics of Phototropin 2 LOV2 Domain with the Linker upon Photoexcitation

EITOKU, Takeshi[1]; NAKASONE, Yusuke[1]; MATSUOKA, Daisuke[2]; TOKUTOMI, Satoru[2]; TERAZIMA, Masahide[3]
([1]Kyoto Univ.; [2]Osaka Pref. Univ.; [3]IMS and Kyoto Univ.)

[*J. Am. Chem. Soc.* **127**, 13238–13244 (2005)]

Conformational dynamics of LOV2 domain of phototropin, a plant-blue-light photoreceptor, is studied by the pulsed laser induced transient grating (TG) technique. The TG signal of LOV2 without the linker part to the kinase domain exhibits the thermal grating signal due to the heat releasing from the excited state and a weak population grating by the adduct formation. The diffusion coefficients of the adduct product after forming the chemical bond between the chromophore and Cys residue is found to be slightly smaller than that of the reactant, which fact implies that the core shrinks slightly on the adduct formation. After that change, no significant conformational change was observed. On the other hand, the signal of LOV2 with the linker part to the kinase domain clearly shows very different diffusion coefficients between the original and the adduct species. The large difference indicates significant global conformational change of the protein moiety upon the adduct formation. More interestingly, the diffusion coefficient is found to be time dependent in the observation time range. This dynamics representing the global conformational change is a clear indication of a spectral silent intermediate between the excited triplet state and the signaling product. From the temporal profile analysis of the signal, the rate of the conformational change is determined to be 2 ms.

II-F Controllable Magnetic Properties of Ultrathin Magnetic Films Using Surface Chemical Techniques

Noble properties of magnetic thin films such as perpendicular magnetic anisotropy (PMA) and giant magentoresistance (GMR) have extremely attracted scientific and technological interests. The origin of perpendicular magnetic anisotropy of ultrathin metal films is not fully understood and is an important subject in fundamental physics but is useful for high-density recording media. The GMR property is already utilized for read-heads of hard disk drives, although quantitative understanding of the GMR is still to be improved. We have been investigating drastic changes of magnetic properties of ultrathin metal films by using surface chemical modification such as atoms/molecules adsorption on the surface. Especially, the microscopic mechanism of spin reorientation transitions induced by gaseous adsorption on magnetic film surfaces have been investigated by means of the synchrotron radiation x-ray magnetic circular dichroism (XMCD), the visible-light magneto-optical Kerr effect (MOKE) and the magnetization induced second harmonic generation (MSHG) techniques. A goal of these works is spin engineering by which the magnetization of ultrathin metal films and nanowires can be controlled artificially.

II-F-1 MOKE and XMCD Study on K Adsorption on Fe Ultrathin Films on Cu(001)

NAKAGAWA, Takeshi; WATANABE, Hirokazu; YOKOYAMA, Toshihiko

It is interesting to investigate whether electron donation to magnetic metal films induces the enhancement or suppression of magnetization. Especially, Fe could be a candidate whose magnetization is enhanced by electron donation. In the present work, we have studied the effect of K adsorption on *fct* (face-centered-tetragonal) Fe and Co grown on Cu(001) by means of the polar MOKE and the XMCD methods.

Figure 1 shows the MOKE intensity from 3 ML Fe on Cu(001) as a function of K coverage, which was measured during K deposition. With the increase in the K coverage, the MOKE intensity increases and at 0.1 ML K deposition it is maximized. More deposition leads to the suppression. The K coverage of 0.1 ML roughly corresponds to the work function minimum. Although the MOKE intensity is usually proportional to the magnetization, it could not be the case if the electronic structure changes drastically. In order to confirm the enhanced magnetization and to obtain more direct information, we have performed XMCD measurements at BL4B of UVSOR-II. Figure 2(a) shows the Fe *L*-edge XMCD. A small increase in the XMCD signals is actually found at the K coverage of 0.1 ML. Table 1 summarizes the results of the quantitative analysis. In both the Fe and Co cases, the number of 3*d* holes, which was estimated from the intensity of the white lines, is gradually reduced with the K coverage, this exemplifying the electron donation from K. In the Co case, the spin magnetic moment decreases monotonically with the K coverage. This finding is reasonable since the majority 3*d* band of *fcc* Co is fully occupied and the donated electron is transferred to the minority 3*d* bands, leading to the reduction of the spin magnetic moment of Co. On the contrary, the spin magnetic moment of Fe is maximized at 0.1 ML K. This verifies that the Fe spin magnetic moment is enhanced by a small amount of K deposition.

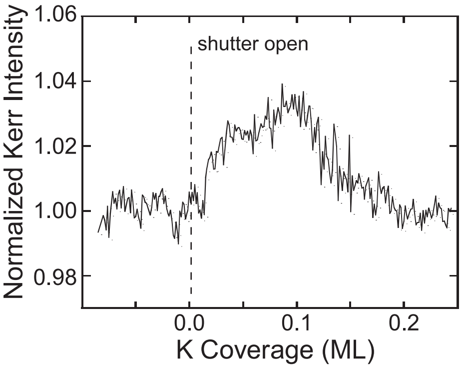

Figure 1. Polar MOKE intensity of 3 ML Fe/Cu(001) at 100 K as a function K deposition.

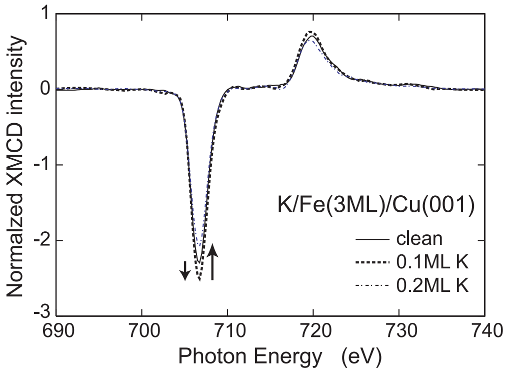

Figure 2. Fe *L*-edge XMCD of 3 ML Fe/Cu(001) (perpendicularly magnetized) at 100 K for the K coverages of 0.0, 0.1 and 0.2 ML.

Table 1. The results of the sum-rule analysis for 3 ML Fe and Co on Cu(001). 3*d* hole numbers and spin (m_s) and orbital (m_l) magnetic moments of Fe and Co are given.

	K dep. (ML)	$3d_{\mathrm{hole}}$ number	m_s (μ_B)	m_l (μ_B)
3 ML Fe /Cu(001)	0.0	3.40	2.29	0.24
	0.1	3.27	2.40	0.24
	0.2	3.00	1.91	0.17
3 ML Co /Cu(001)	0.0	2.50	1.67	0.26
	0.1	2.37	1.58	0.26
	0.2	2.27	1.50	0.29

II-F-2 Spin Reorientation Transition in Ag-Covered Co Films Grown on Vicinal Cu(001) Surface Studied by Means of XMCD

NAKAGAWA, Takeshi; WATANABE, Hirokazu; YOKOYAMA, Toshihiko

Magnetic thin films grown on vicinal surfaces exhibit strong uniaxial magnetic anisotropy; the magnetic property should be essentially different between the step-parallel and perpendicular directions. In this work, in order to obtain microscopic information on the spin reorientation transition in Ag-deposited Co films on Cu(1 1 17), we performed the longitudinal MOKE and XMCD experiments.

Figure 1 shows the magnetic hysteresis loops of MOKE. In the clean Co film, the magnetization curve along the //step direction exhibits normal rectangular shape, while that along the ⊥step direction shows a double loop with zero remanence, this implying the easy axis of the //step direction. On the contrary, the reverse is true for the 0.2 ML Ag-deposited Co film; the magnetic easy axis changes from //step to ⊥step, exhibiting clear spin reorientation transition. This results is identical with the previously reported work by Weber *et al.* [*Phys. Rev. B* **52**, R14400 (1995)].

Figure 2 shows the Co *L*-edge XMCD. The intensities of the L_{III}- and L_{II}-edge peaks exhibit clear difference between the clean and Ag-deposited Co films. Although the difference is rather small, one can find that larger orbital magnetic moments give the magnetic easy axis from the detailed sum-rule analysis: for clean Co, $m_l^{//} = 0.246\ \mu_B$ and $m_l^{\perp} = 0.225\ \mu_B$, while for Ag-deposited Co, $m_l^{//} = 0.200\ \mu_B$ and $m_l^{\perp} = 0.218\ \mu_B$. Moreover, we have determined the inclination angle of the easy axis. Figure 3 shows the results of the XMCD variation. The *x*-intercept corresponds to the easy axis, where 0° and –4.8° respectively mean parallel to the physical plane and to the terrance plane. The present finding in Figure 3 concludes that the Ag deposition induces also the out-of-plane rotation of the easy axis from the physical surface plane (0°) to the terrance plane (–4.8°).

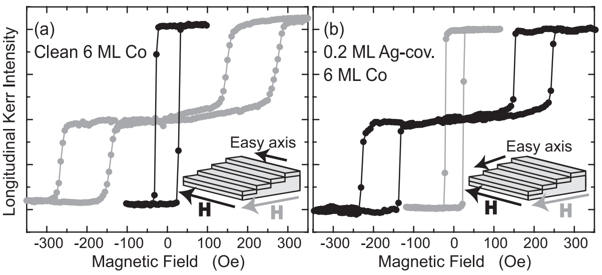

Figure 1. MOKE hysteresis loops of (a) clean and (b) Ag-deposited 6 ML Co/Cu(1 1 17) at 100 K.

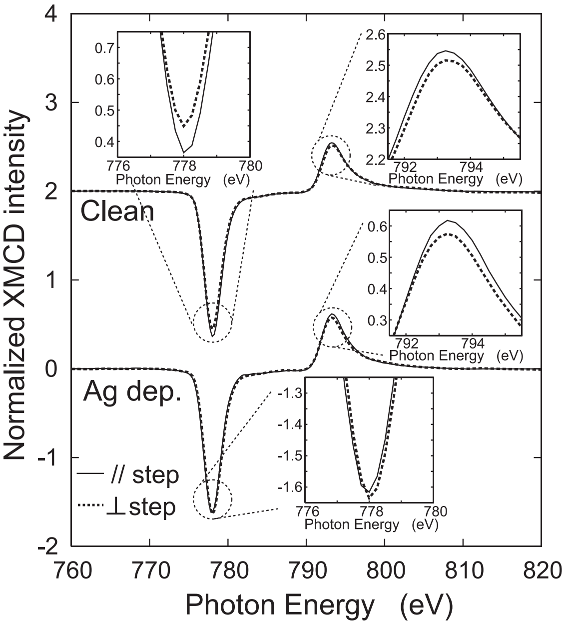

Figure 2. Co *L*-edge XMCD of 6 ML Co/Cu(1 1 17) at 100 K before and after 0.2 ML Ag deposition.

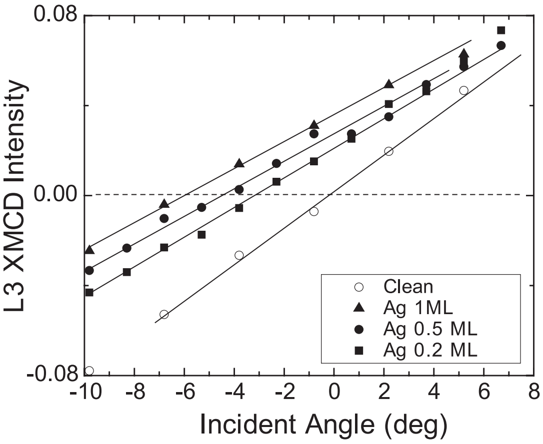

Figure 3. Angle dependence of Co L_{III}-edge XMCD intensity of 6 ML Co/Cu(1 1 17).

II-F-3 Drastic Magnetization Change Observed in NO Adsorption on Co/Cu(1 1 17)

NAKAGAWA, Takeshi; WATANABE, Hirokazu; YOKOYAMA, Toshihiko

Magnetic thin films grown on vicinal surfaces exhibit strong uniaxial magnetic anisotropy and the anisotropy could be modified by surface chemical treatments. In this work, we have investigated the effect of NO adsorption on uniaxial Co films grown on Cu(1 1 17) by means of the longitudinal MOKE and the XMCD experiments.

Figure 1 shows the magnetic hysteresis loops of longitudinal MOKE. In the clean Co film, the magnetization curve along the //step direction exhibits normal rectangular shape, while that along the ⊥step direction shows a double loop with zero remanence, this implying the presence of strong uniaxial magnetic anisotropy and the easy axis of the //step direction. However, drastic changes can be seen after NO adsorption. The coercivity is reduced noticeably, and the //step and ⊥step loops are completely identical, this indicating the disappearance of the inherent uniaxial anisotropy and the appearance of almost fourfold symmetric magnetic anisotropy. Such a change is much more drastic than the film on flat Cu(001).

Figure 2 shows the Co *L*-edge XMCD. The intensities of the L_{III}- and L_{II}-edge peaks exhibit clear difference between the clean and NO-adsorbed Co films. From the detailed sum-rule analysis, one can find that in a clean Co film a larger orbital magnetic moments give the magnetic easy axis (for clean Co, $m_l^{//} = 0.256\ \mu_B$ and $m_l^{\perp} = 0.224\ \mu_B$), while the orbital magnetic moments are essentially the same between the //step and ⊥step directions after NO adsorption ($m_l^{//} = 0.116\ \mu_B$ and $m_l^{\perp} = 0.123\ \mu_B$). This is consistent with the longitudinal MOKE results.

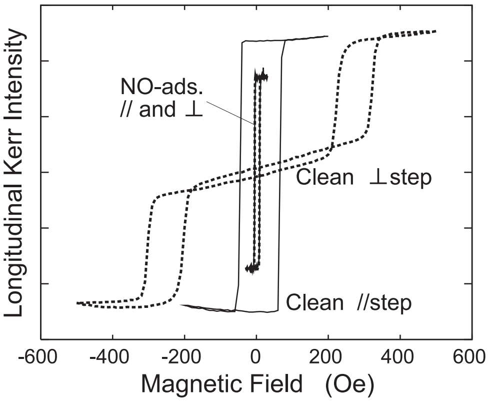

Figure 1. Longitudinal MOKE hysteresis loops of clean and NO-adsorbed 6 ML Co films on Cu(1 1 17) at 100 K.

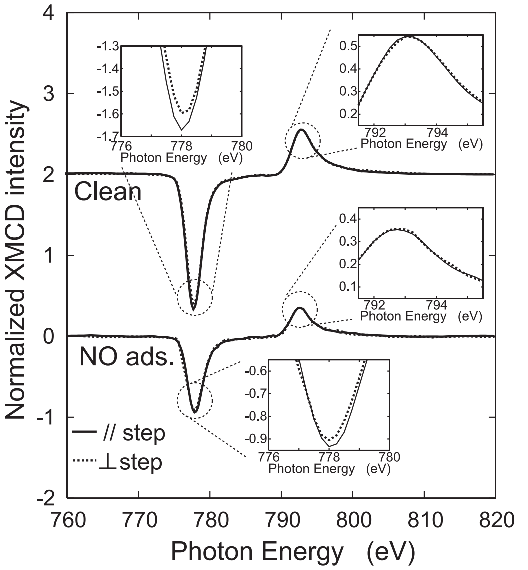

Figure 2. Co *L*-edge XMCD of 6 ML Co/Cu(1 1 17) at 100 K before and after 0.5 ML NO adsorption.

II-F-4 Direct Observation of Biquadratic Exchange Interaction in Fe/Ni/Cu(001) by Using MSHG

NAKAGAWA, Takeshi; YOKOYAMA, Toshihiko

Ultrathin *fcc* Fe films are known to exhibit various peculiar magnetic properties since *fcc* Fe shows ferromagnetism and antiferromagnetism depending on very small changes in the lattice constant. Very recently, Liu *et al.* [*Phys. Rev. B* **65** 224413 (2002)] observed an exchange bias in Fe/Ni/Cu(001) from their MOKE measurements and proposed that in there should exist biquadratic exchange interaction (perpendicular spin-spin interaction is stable). This observation is quite interesting since in the Fe/Ni system all the magnetic metal atoms are directly bonded with each other and Heisenberg exchange interaction is usually expected. In this work, we have obtained direct proof for the perpendicular magnetization in this system by using the MSHG technique exploited in this group.

Figure 1 shows the longitudinal MOKE and MSHG results. The curves of MOKE and MSHG Pin-Sout (S-polarization incidence and P-polarization reflection) give the magnetization along the magnetic field, while those of Pin-Pout and Sin-Pout the magnetization perpendicular to the magnetic field within the film plane. Actually, the perpendicular components are observed especially for 3.3 ML Fe. Figure 2 shows the remanent magnetization and the coercive field as a function of Fe coverage. Two minima at ~4 and ~8 ML Fe can be seen. We can recognize that each Fe layer interacts with the adjacent layer so that the magnetization directions are perpendicular with each other; 4 and 8 ML Fe films correspond to one and two periodic antiferromagnets, respectively. The presence of the biquadratic exchange interaction in this system is experimentally proved.

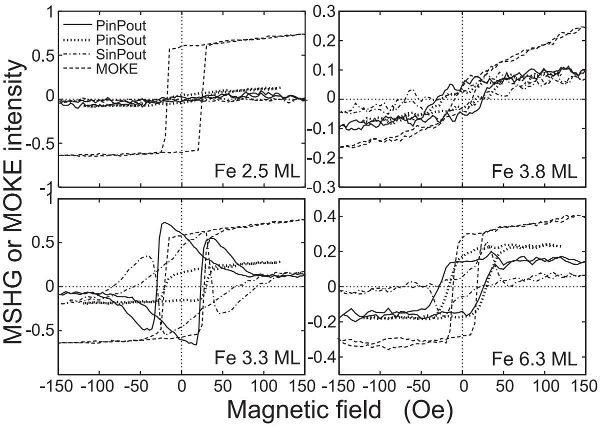

Figure 1. Magnetization curves given by the longitudinal MOKE and the MSHG (Pin-Pout, Sin-Pout and Pin-Sout) for Fe/Ni(7 ML)/Cu(001).

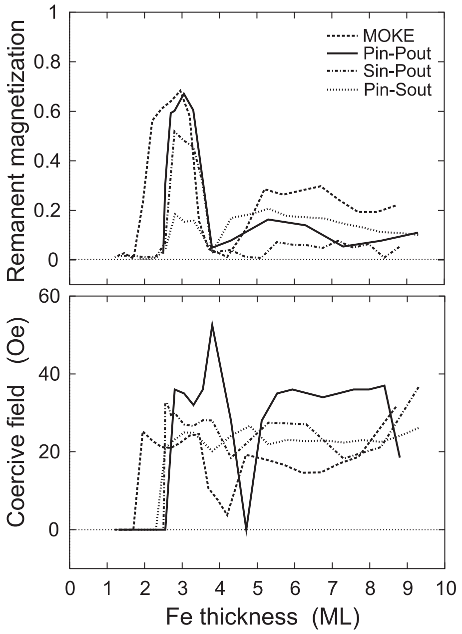

Figure 2. Remanent magnetization and the coercive field as a function of Fe coverage given by the longitudinal MOKE and the MSHG.

II-G Local Structures of Molecular-Based Magnetic Materials Studied by X-Ray Absorption Fine Structure Spectroscopy

Molecular-based magnets provide noble properties such as quantum tunneling of magnetization, photoinduced magnetism *etc.* In order to understand fully the magnetic properties, structural information is indispensable. Although usually the X-ray diffraction analysis of single crystals is the most appropriate to determine the three-dimensional structure, there exist several cases when the X-ray diffraction analysis cannot be applied: the crystal structure is disordered, single crystals are hardly obtainable, and so forth. We have been studying local structures and electronic properties of interesting molecular magnets by means of X-ray absorption fine structure (XAFS) spectroscopy.

II-G-1 Molecular Structure of Single-Molecule Magnet $Mn_{11}Cr$, $Mn_{11}Cr^{-}$ and $Mn_{10}Fe_2$

YOKOYAMA, Toshihiko; HACHISUKA, Hidekazu[1]; AWAGA, Kunio[1]
([1]Nagoya Univ.)

[*Phys. Rev. B* **70**, 104427 (2004)]

Single-molecular magnet of $[Mn_{12}(AcO)_{16}(H_2O)_4]$ (Ac = CH_3COO) has extensively been investigated because of its interesting properties such as stepwise magnetization due to the quantum tunneling effect. One of the outstanding features of molecular magnets is the ease of chemical modification. Recently, molecular magnets of $Mn_{11}Cr$ ($[Mn_{11}CrO_{12}(AcO)_{16}(H_2O)_4]$) $Mn_{10}Fe_2$ ($[Mn_{10}Fe_2O_{12}(AcO)_{16}(H_2O)_4]$) and $Mn_{11}Cr^{-}$ ($[(Ph)_4P][Mn_{11}CrO_{12}(PhCOO)_{16}(H_2O)_4]$) were synthesized. Although the single crystal x-ray diffraction analyses have been performed, the location of Cr or Fe cannot be determined because of the crystalline disorder of their positions. In such a case, EXAFS is the most suitable technique to determine the molecular structure.

Figure 1 depicts the Fourier transforms of the EXAFS functions of $Mn_{11}Cr$. The x-ray molecular structure gives the average structure where Cr is not distinguished from Mn. There exist three types of Cr/Mn sites: Sites **1**, **2**, and **3**, as shown in Figure 2. Site **1** is occupied by Mn^{4+} ions, while Sites **2** and **3** are by Mn^{3+}. The Fourier transform of Cr is similar to the simulated one of Site **3**. It is thus concluded that, in $Mn_{11}Cr$, Cr^{3+} exclusively occupies Site **3**, the tilted site for Mn^{3+} in the Mn_{12} skeleton. The magnitude of the experimental Cr–O peak is much stronger than that of the theoretical one of Site **3**, because the Mn^{3+} ion in Site **3** exhibits significantly distorted octahedron due to the Jahn-Teller effect, resulting in the suppression of the Mn–O contribution in the simulation. On the contrary, the Cr^{3+} ion shows no Jahn-Teller distortion, yielding more intense Cr–O contribution in the Fourier transform.

Essentially the same results are obtained for $Mn_{10}Fe_2$ and $Mn_{11}Cr^{-}$, and in conclusion, the Cr/Fe ion locates exclusively at Site **3** with normal valency of Cr/Fe(III).

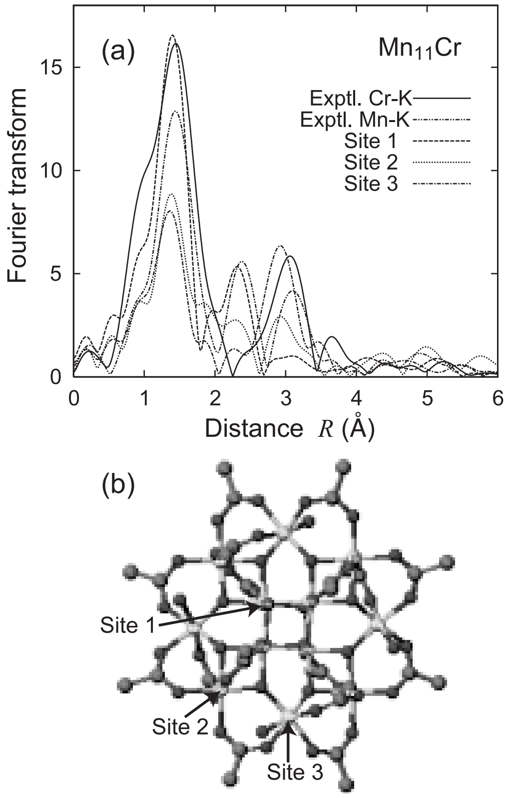

Figure 1. (a) Fourier transforms of the Cr (solid line) and Mn (dot-dot-dashed) K-edge EXAFS functions, together with the theoretical simulation results for Sites **1** (dotted), **2** (dot-dashed) and **3** (dashed). (b) Molecular structure of Mn_{12}. Mn atoms locate three inequivalent Sites **1**, **2** and **3**.

II-G-2 Photoinduced Phase Transition of CuMo Cyanides Studied by XAFS Spectroscopy

MA, Xiao-Dong; YOKOYAMA, Toshihiko; HOZUMI, Toshiya[1]; HASHIMOTO, Kazuhito[1]; OHKOSHI, Shin-ichi[1]
([1]Univ. Tokyo)

[*Phys. Rev. B* **72**, 094107 (2005)]

Prussian-blue analogues often exhibit noble magnetic properties such as photoinduced magnetization. In this work, we have investigated the local structures and the electronic states mainly of the photoinduced phases of two CuMo cyanides of $Cu_2Mo(CN)_8{\cdot}8H_2O$ (**1**) and $Cs_{0.5}Cu_{1.75}Mo(CN)_8{\cdot}1.5H_2O$ (**2**) by means of XAFS. Usually, the photoinduced phase at low temperature is considered to be structurally identical to that of the corresponding high-temperature phase. However the photoinduced phase is an essentially new state for these two CuMo compounds because in the low-temperature phase even at room temperature they are likely to decompose with the temperature rise before thermally driven phase transition takes place.

Figure 1(a) shows the Cu *K*-edge spectra of samples (**1**) and (**2**) before and after photoirradiation, together with the reference spectra of $Cu^{(I)}{}_2O$ and $Cu^{(II)}O$. One can immediately conclude that the Cu atoms in samples (**1**) and (**2**) are divalent before photoirradiation, and monovalent Cu appears after photoirradiation. Figure 1(b) shows the Mo and Cu *K*-edge EXAFS Fourier transforms of sample (**2**). Overall, one can find that the features of the initial low-temperature and photoinduced phases are almost identical. The interatomic distances are almost the same between the initial and the photoinduced phases. Differences between the low-temperature and the photoinduced phases can however be detected in the amplitude in the EXAFS oscillation. The coordination numbers of the Mo–N, Mo–Cu, and Cu–Mo shells are found reduced, while those of the Mo–C, Cu–N, and Cu–C shells as well as the first-nearest neighbor Mo–C and Cu–N shells are kept constant. The latter implies enhancement of the static Debye-Waller factors. The reduction of the coordination numbers for the Mo–N, Mo–Cu, and Cu–Mo shells may be ascribed not to the bond breaking but to the bond bending. One can qualitatively conclude that due to the photoirradiation the Mo–CN bond is bent, while the Cu–NC bond angle is kept unchanged.

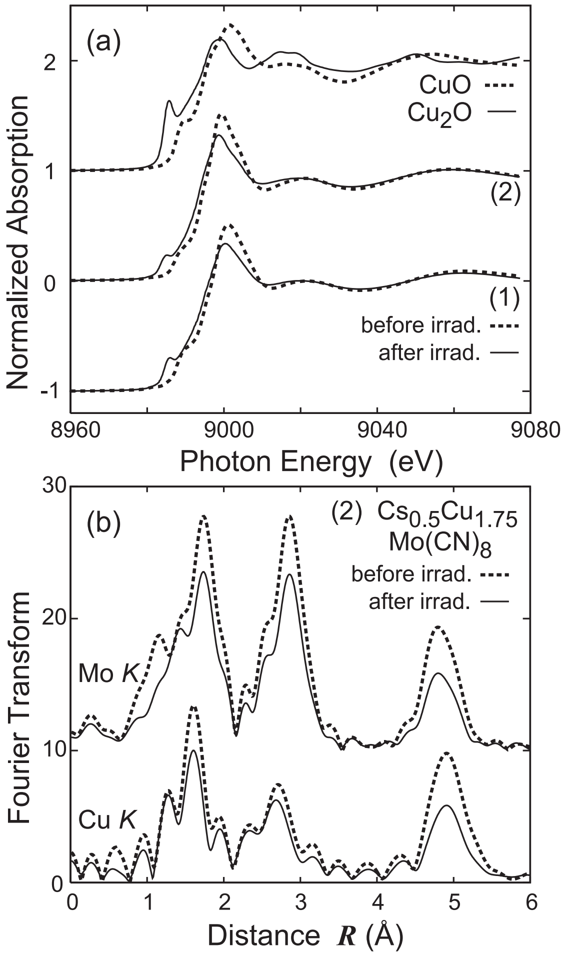

Figure 1. (a) Cu *K*-edge X-ray absorption spectra of samples (**1**) and (**2**), together with those of Cu_2O and CuO. (b) Fourier transforms of the Mo and Cu *K*-edge EXAFS oscillation functions of sample (**2**) at 30 K before and after photoirradiation.

II-H Development of Fluorescent and Bioluminescent Proteins for Imaging Intracellular Molecular Dynamics

A current focus of biological researches is to quantify and image cellular events in living cells and animals. To probe the fundamental cellular events in living cells, we are exploring a new way for developing fluorescent and bioluminescent reporter proteins based on protein splicing. With these reporter proteins, analytical methods to detect protein-protein interactions, intracellular localization of proteins and their dynamics, enzyme activities, gene expression, and production of small bio-molecules are being actively under development. We are also investigating analytical techniques such as complementary DNA library screenings and proteome analysis.

II-H-1 Quantitative Determination of Protein Nuclear Transport Induced by Phosphorylation or by Proteolysis

KIM, Sung Bae[1]; TAKAO, Ryohei[1]; OZAWA, Takeaki; UMEZAWA, Yoshio[1]
(*[1]Univ. Tokyo)*

[*Anal. Chem.* **77**, 6928–6934 (2005)]

Nucleocytoplasmic transport of proteins in eukaryotic cells is a fundamental process for gene expression. The transport is regulated by post-translational modifications of the proteins such as ligand-binding, phosphorylation, and proteolysis. For monitoring the nuclear transport of proteins induced by a ligand binding, we have recently developed a genetically-encoded bioluminescent indicator based on reconstitution of split fragments of *Renilla reniformis* (Rluc) by protein splicing of a DnaE intein.1) We herein describe that the technique is used for detecting phosphorylation- or proteolysis-induced nuclear transports of a target protein. Two model proteins, signal transducer and activator of transcription 3 (STAT3) and sterol-regulatory element binding proteins-2 (SREBP-2), were exemplified as phosphorylation- and proteolysis-induced nuclear transport, respectively. Each STAT3 or SREBP-2 is connected with C-terminal halves of Rluc and DnaE. If the protein translocates into the nucleus, the C-terminal Rluc meets the N-terminal Rluc, and full-length Rluc is reconstituted by protein splicing in the nucleus. The indicator with SREBP-2 enabled to quantify the intracellular concentrations of cholesterol. The indicator with STAT3 quantified the extent of the nuclear transport induced by representative cytokines. This simple assay based on protein nuclear transports allows the selection of suitable drugs among candidates, and has significant potential for risk assessments such as carcinogenic chemical screening *in vitro* and *in vivo*.

Reference

1) S. B. Kim, T. Ozawa, S. Watanabe and Y. Umezawa, *Proc. Natl. Acad. Sci. U.S.A.* **101**, 11542–11547 (2004).

II-H-2 A Stress Indicator for Noninvasively Imaging Endogenous Corticosterone in Living Mice

KIM, Sung Bae[1]; OZAWA, Takeaki; UMEZAWA, Yoshio[1]
(*[1]Univ. Tokyo)*

[*Anal. Chem.* **77**, 6588–6593 (2005)]

The physical and emotional stress is one of the major controllers of physiological reactions and homeostasis in living animals. A stress hormone, corticosterone, is secreted from adrenal cortex into the blood vessel when animals sense the stress. The quantitative evaluation of corticosterone in living animals has been limited because of the unavailability of suitable methods *in vivo*. For a noninvasive molecular imaging of the stress, we developed a method for detecting physiological increases in the endogenous corticosterone caused by exo- and endogenous stress in living animals. We constructed a pair of genetically-encoded indicators composed of cDNAs of glucocorticoid receptor (GR), split *Renilla* luciferase (RLuc) and a *Synechocystis* sp. DnaE intein. The GR fused with C-terminal halves of RLuc and DnaE is localized in the cytosol, whereas a fusion protein of N-terminal halves of RLuc and DnaE is localized in the nucleus. If corticosterone induces GR translocation into the nucleus, the C-terminal RLuc meets the N-terminal one in the nucleus, and full-length RLuc is reconstituted by protein splicing with DnaE. Cell-based methods provided quantitative bioluminescence assay of the extent of GR translocation into the nucleus. We further demonstrated that the indicator enabled noninvasive imaging against two different types of imposed stress: a forced swimming and metabolic perturbation caused by 2-deoxy-D-glucose. This stress indicator should be valuable for screening pharmacological compounds and for tools to study the mechanism of physiological stress.